This is a repository copy of *A versatile, pulsed anion source utilizing plasma-entrainment: Characterization and applications*.

Article:

A versatile, pulsed anion source utilizing plasma-entrainment: Characterization and applications

Yu-Ju Lu, Julia H. Lehman, and W. Carl Lineberger

Articles you may be interested in

Velocity map imaging of ions and electrons using electrostatic lenses: Application in photoelectron and photofragment ion imaging of molecular oxygen
Review of Scientific Instruments **68**, 3477 (1997); 10.1063/1.1148310

Anion photoelectron spectroscopy of deprotonated ortho-, meta-, and para-methylphenol
The Journal of Chemical Physics **146**, 074302 (2017); 10.1063/1.4975330

Finite slice analysis (FINA)—A general reconstruction method for velocity mapped and time-sliced ion imaging
The Journal of Chemical Physics **147**, 013913 (2017); 10.1063/1.4979305

Photoelectron spectroscopy of the hydroxymethoxide anion, $H_2C(OH)O^-$
The Journal of Chemical Physics **145**, 124317 (2016); 10.1063/1.4963225

Perspective: Electrospray photoelectron spectroscopy: From multiply-charged anions to ultracold anions
The Journal of Chemical Physics **143**, 040901 (2015); 10.1063/1.4927086

Photodissociation spectroscopy and dynamics of the $N_2O_2^-$ anion
The Journal of Chemical Physics **104**, 5026 (1996); 10.1063/1.471132
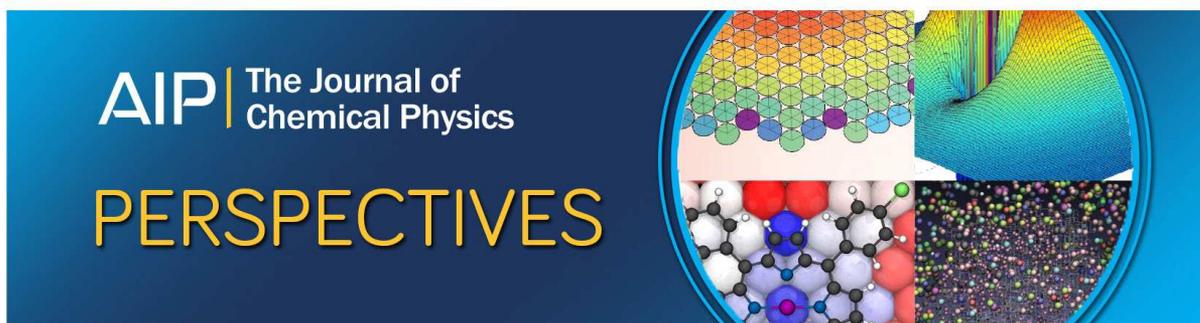
A versatile, pulsed anion source utilizing plasma-entrainment: Characterization and applications

Yu-Ju Lu, Julia H. Lehman, and W. Carl Lineberger[a)]
JILA and Department of Chemistry and Biochemistry, University of Colorado, Boulder, Colorado 80309, USA

A novel pulsed anion source has been developed, using plasma entrainment into a supersonic expansion. A pulsed discharge source perpendicular to the main gas expansion greatly reduces unwanted "heating" of the main expansion, a major setback in many pulsed anion sources in use today. The design principles and construction information are described and several examples demonstrate the range of applicability of this anion source. Large $OH^-(Ar)_n$ clusters can be generated, with over 40 Ar solvating OH^-. The solvation energy of $OH^-(Ar)_n$, where n = 1-3, 7, 12, and 18, is derived from photoelectron spectroscopy and shows that by n = 12-18, each Ar is bound by about 10 meV. In addition, *cis*– and *trans*– $HOCO^-$ are generated through rational anion synthesis ($OH^- + CO + M \rightarrow HOCO^- + M$) and the photoelectron spectra compared with previous results. These results, along with several further proof-of-principle experiments on solvation and transient anion synthesis, demonstrate the ability of this source to efficiently produce cold anions. With modifications to two standard General Valve assemblies and very little maintenance, this anion source provides a versatile and straightforward addition to a wide array of experiments. © *2015 AIP Publishing LLC.* [http://dx.doi.org/10.1063/1.4906300]

I. INTRODUCTION

Negative ion photoelectron spectroscopy has been widely applied to investigate the spectroscopic properties of neutral species[1–3] and the dynamics of photodissociation,[4,5] cage recombination,[6,7] S_N2 reactions,[8] isomerization,[9] and charge transfer.[10,11] In order to study such an extensive array of photochemical processes and reaction dynamics, a variety of anion sources have been developed for both continuous wave (cw) and pulsed instruments, the latter of which is the focus of this investigation.

A pulsed anion beam is typically constructed using a pulsed supersonic jet which is coaxially or perpendicularly intersected with a continuous beam of 1 keV electrons from an electron gun.[12] For the formation of some anions, an electrical discharge source[13–16] or a laser vaporization source[17–20] is required, either of which can result in a high temperature environment. These common pulsed sources use the main pulsed expansion in which to create ions. In general, collisions with an atomic carrier gas in a supersonic expansion lead to sufficient cooling of the internal degrees of freedom for high-resolution spectroscopic applications. However, a gas expansion that passes through or is responsible for the generation of a hot plasma contains too many energetically excited neutral species to completely cool the anions formed. The insufficient internal cooling of anions in the supersonic jet from rovibrational excitation produces broad and/or dense photoelectron spectra, limiting the ability to extract spectroscopic information.

To prevent this, several methods for cooling anions generated in a hot source have become common. For example,

Ar-tagging[21,22] uses a supersonic entrainment technique to attach Ar solvent atoms to anions and build large complexes. Additional neutral solvents can be added through the entrainment source, such as in the supersonic afterglow reactor developed by Johnson and coworkers[22] or the cw combined plasma and "pick-up" line ion source from Bowen and coworkers.[23,24] Since Ar atoms weakly bind to anions, mass selecting for anion-Ar clusters limits the internal energy of the anion, suppressing hot bands and reducing spectral congestion.[25–28] However, more than simply cooling the hot anions will be essential if the goal is to synthesize anions of interest via rational multistep synthetic methods.

Cryogenic ion trapping has also been used with great success to generate cold anions from an initially hot ion source.[29,30] These ions can be mass-selected, stored, and cooled in a cryogenic ion trap via collisions with a cold buffer gas before being extracted for further spectroscopic measurements. Cryogenic ion trapping has been coupled to electrospray ionization (ESI) sources to transfer ions from solution into the gas phase and efficiently cool the numerous internal degrees of freedom of large species.[31–34] While ESI is a soft-ionization technique to generate large (macromolecular) gas phase ions, these ions must have already been stable in solution. In addition, it is difficult to initiate and control chemical reactions for production of new species. The new source described here should be viewed as a complement to the ESI/cryogenic ion trapping source, in that it is able to address different subsets of ions: both of those whose neutral counterpart is either already in the gas phase or has a high vapor pressure, as well as the ability to generate transient ion species through rational synthesis, a unique feature of this new ion source.

This ion source is essentially an entrainment source, similar to those already discussed. However, the main expansion

---

a)Email: wcl@jila.colorado.edu

is not used directly as the ion source and entrainment is not limited to neutral species. Instead, plasma generated in a violent, high-energy environment in a side discharge expansion is entrained into the region of high density of a second (main) expansion. The design of the side discharge preferentially injects plasma into the primary expansion, minimizing entrainment of hot neutral molecules, which facilitates efficient cooling of the injected charged particles. The capabilities of this novel source are explored here, such as electron and ion entrainment, solvation or tagging, and rational ion synthesis, demonstrating its versatility. While the production of anionic species is shown, this source can likely be used for cation production as well. This new source addresses many of the previous drawbacks or difficulties present in other current pulsed anion sources, particularly the difficulty of efficient cooling and generating transient species through rational chemical means, while being adaptable to many types of experiments, low-maintenance, and straightforward to construct.

II. EXPERIMENTAL SETUP AND ION SOURCE CHARACTERIZATION

Beyond the new ion source, which is discussed below, the remaining aspects of the experimental apparatus have been described in detail elsewhere.[35] Briefly, ions are perpendicularly extracted into a Wiley-McLaren time-of-flight (TOF) mass spectrometer, where they are accelerated, steered, and focused onto an inline microchannel plate (MCP) detector, yielding the TOF mass spectra reported herein. Prior to the inline detector, the interaction of the anion mass of interest with an appropriately timed laser pulse detaches electrons. A pulsed electric field, which constitutes the first stage of a velocity map imaging setup,[36,37] then accelerates the electrons perpendicular to the molecular beam axis. The electrons are velocity mapped onto a MCP/phosphor screen coupled to a CCD camera. The

resulting photoelectron image is converted to a kinetic energy distribution following inverse Abel transformation through the BASEX algorithm.[38] The kinetic energy distribution is related to the electron binding energy (eBE) through the photon energy used. The photoelectron spectra reported herein are shown as a function of the electron binding energy.

Figure 1 shows a schematic of the new pulsed anion source. The setup employs two pulsed General Valves (Parker-Hannifin, Series 9): one that functions to generate the main expansion and the other, oriented perpendicular and very close to this main expansion, utilizes a pulsed electrical discharge. Since the two valves are independently controlled by a commercial multi-channel Iota-One pulse driver and a digital delay generator, temporal overlap of the two gas pulses can be adjusted in real time.

The main valve operates under "normal" pulsed supersonic jet expansion conditions. Typical pulse widths and backing pressures are in the range of 110-160 μs and 40 psig, respectively. The backing gas composition varies, depending on the experiment. However, since efficient cooling is necessary for the examples discussed herein, Ar is the primary component of the main gas expansion. The main valve assembly is altered from the standard General Valve assembly by replacing the standard faceplate with a modified one, shown schematically in Fig. 1 and in detail in the Supplementary Material.[39] The outer diameter of the faceplate is reduced in order to allow the second nozzle to be situated much closer than what was previously possible, with a distance of approximately 13 mm between the front of the side valve assembly and the orifice of the main valve faceplate, as shown in Fig. 1. In addition, in order to increase the forward intensity of the main expansion, a 40° conical nozzle with a 0.5-mm orifice (D_O) and an aspect ratio (L/D_O) of 7 was designed.[40] While this last modification is not necessarily crucial to the anion source, the enhanced collimation of the main expansion does aid in
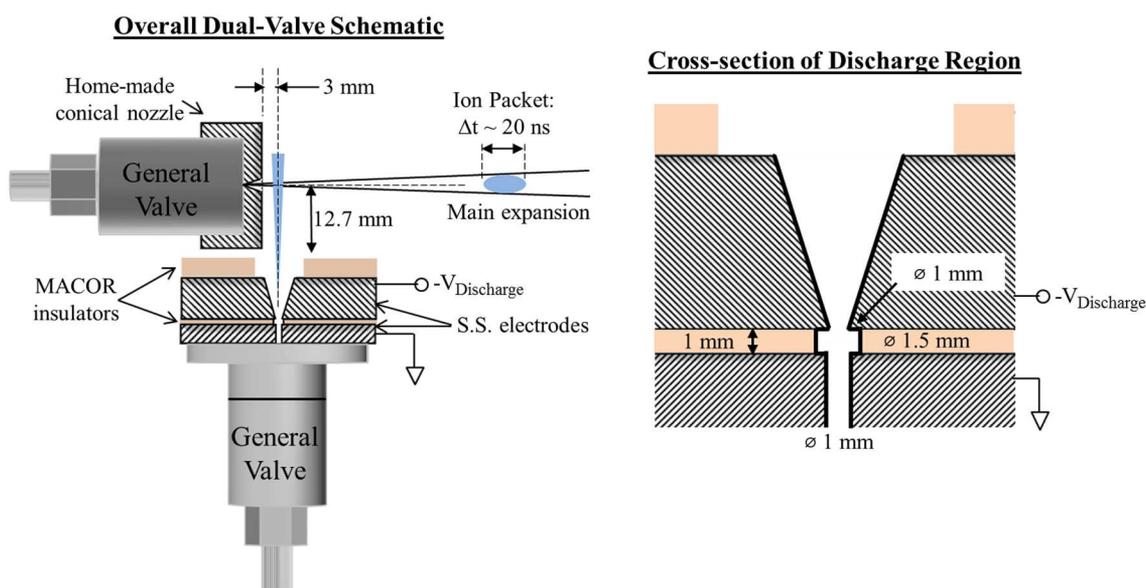
FIG. 1. Schematic arrangement of the pulsed plasma-entrainment anion source employing two solenoid valves. The home-made components are presented in further detail in the Supplementary Material.[39] The inset shows a larger cross section of the small (1.5 mm in diameter) discharge region between the two electrodes separated by the 1 mm thick MACOR insulator.

improving the overall performance of this source. The new faceplate seals in the same manner as the commercial faceplate and, thus, couples with the unmodified General Valve body.

The side valve operates under mechanically limited valve opening conditions, where the gas throughput per pulse is roughly one order of magnitude less than that from the main valve. For example, above a source chamber base pressure of around 5×10^{-6} Torr, the operating pressure with the main valve firing is approximately 2.8×10^{-5} Torr and approximately 3.1×10^{-5} Torr with both valves firing (50 Hz repetition rate, source chamber vacuum achieved with a 10 in. oil diffusion pump having an approximate 4000 l/s air pumping speed specification). While typical pulse widths and backing pressures are similar to the main expansion, the side valve tension is adjusted to give this performance; both valves operate with the same Iota-One controller drive voltage. The entrainment of the plasma, discussed below, from the side valve into the main supersonic expansion without disruption of the main expansion, relies on the side valve operating under low gas density conditions, making this setup specification crucial to the functionality of the ion source.

The pulsed discharge assembly is attached to an unmodified side valve faceplate (General Valve, 0.8 mm orifice). It is comprised of two electrodes, where the one adjacent to the faceplate is held at ground and the other is pulsed to a high negative voltage; a cylindrical MACOR plate insulates the two electrodes from each other. A second MACOR ring is added to the end of the whole assembly. While the electrodes used for the majority of the work presented here are stainless steel, an aluminum cathode has also been used, primarily for discharging halogen-containing compounds or for use with lower (below -1000 V) pulsed voltages. The dimensions of the discharge assembly are shown in detail in the Supplementary Material.[39]

A pulsed voltage between -500 and -2000 V is used to maximize the ion intensities and the stability of the discharge. The negative voltage pulse is provided by a pulse generator (Directed Energy, Inc. (DEI), GRX-3.0K-H or PVX-4140) with a DC power supply (Bertan associates, Inc., 205-03R or Kepco ABC 2500). The pulser is triggered by a digital delay generator which controls the discharge timing and pulse duration (40–140 μs), both of which are adjusted to optimize ion intensities. In addition, a 20 kΩ resistor in series with the cathode acts as a ballast resistor, allowing a high voltage discharge ignition followed by a current regulated, stable discharge. A time trace for the voltage measured across the discharge electrodes for a -2000 V, 85 μs applied discharge pulse is shown in Fig. 2 (red trace), with an inset illustrating the circuit diagram. When this pulse is applied through the 20 kΩ resistor, the voltage drop across the resistor is approximately -1600 V, corresponding to a discharge current of ~ 80 mA (also shown in Fig. 2, blue trace). The ballast resistor depicted allows the roughly -1300 V between the plates to initiate the discharge, but then limits the discharge current to a maximum of 100 mA, providing current regulation and arc suppression.

The spatial volume over which the discharge occurs is very small, as seen in the righthand side of Fig. 1. As the gas expands into the discharge assembly, the breakdown occurs in a small 2 mm^3 annulus between the ground and high voltage
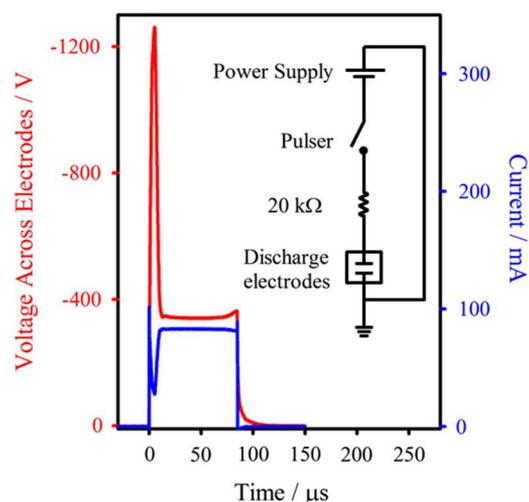
FIG. 2. Voltage and current time traces resulting from a -2000 V, 85 μs applied discharge voltage for OH$^-$ production. Through the 20 kΩ resistor, the voltage drops about 1600 V (red trace), which corresponds to the peak discharge current of 80 mA (blue trace). The inset shows the circuit diagram in which the discharge electrodes are under vacuum in the source chamber.

electrodes, approximately 1.5 mm in diameter and 1 mm thick, made possible by the slightly wider hole through the central MACOR insulator compared to the electrodes. After initiating a discharge in the side expansion, the gas forms a plasma (a neutral medium consisting of many charged particles: electrons, cations, and anions) with a Debye shielding length which is much shorter than the physical dimension of the plasma. However, the charged species of a plasma do not move independently. The slow, heavy ions pull back on the rapidly moving light electrons, creating an ambipolar diffusion that results in the electrons and ions having the same diffusion rate.[41] This diffusion rate is approximately twice that of the free diffusion of the ions, whereas it is substantially less than that of free electrons. As the plasma exits the side discharge, the small degree of its expansion is described by its ambipolar diffusion. Assuming a 200 m/s expansion velocity, the plasma originating from the small annulus would form a 2 cm long plasma "pellet" during a typical 100 μs discharge pulse. By contrast, any hot neutrals that are formed in a typical 120 μs gas pulse of the side valve expand in a near-effusive manner due to the overall low gas density and the construction of the side discharge valve conical aperture.

The confirmation of a plasma being formed is tested through the entrainment of electrons into the main expansion. Electrons not part of a plasma would expand far beyond the size of the main expansion and significant electron entrainment would not be possible. However, with ambipolar diffusion of a plasma, the attachment of slow electrons to neutral molecules in the main expansion is possible. The achievement of electron entrainment in the main expansion is demonstrated by the mass spectra in Fig. 3. Using neat Ar in both the main expansion and the side discharge (-2000 V in a 140-μs discharge pulse), the only ions observed arise from sputtering of the stainless steel discharge plates and are present in most of the mass spectra reported here. Keeping the same neat Ar side discharge and adding a small amount of O_2 to the main expansion (1% O_2 in Ar) creates intense O$^-$ and O_2^- anion signals (red trace
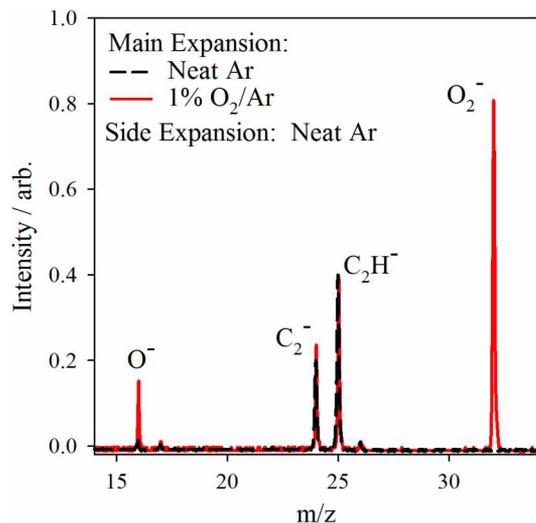
FIG. 3. Comparison between TOF mass spectra from experiments using neat Ar (black dashed) and 1% O_2/Ar (red) for the main expansion. Neat Ar is used in the side discharge source for both experiments. Entrainment of electrons is demonstrated from the formation of the O^- and O_2^- anions. The appearance of small hydrocarbons arises from sputtering of the stainless steel discharge electrodes.

in Fig. 3), which can only arise from electron attachment in the following manner: the O^- is the product of dissociative attachment of hot electrons to O_2, while O_2^- results from collisionally stabilized slow electron attachment to O_2. This ion formation through electron entrainment confirms the generation of a plasma in the side discharge valve. It is important to note that the ion signals obtained here are at least as intense as the other common sources mentioned earlier.

The time spread of the ion packet entrained in the main expansion is measured by varying the timing of the extraction plate that directs anions into the TOF mass spectrometer. Even though both pulsed valve opening times are around 120-140 μs and a long pulsed discharge width (near 100 μs) is used, a significantly smaller time width of the ion packet is measured, where its full-width-at-half-maximum (fwhm) is approximately 20 μs. This indicates a small spatial coverage of ions within the main gas expansion. This ion time width remains approximately constant through all the experiments described below, regardless of the pulsed discharge time width (varied from 40 to 140 μs) and is significantly shorter than the gas pulse widths of the two valves, both larger than 100 μs. The mechanically limited valve opening of the side valve resulting in a low gas density is combined with the narrow spatial region over which the discharge occurs and the ambipolar diffusion holding the plasma together, which likely results in a plasma "pellet" surrounded by near-effusive hot neutrals. The narrow time spread of the ion packet then stems from the spatial and temporal cross section of the plasma "pellet" with the main gas expansion.

The plasma created in the side discharge is introduced into the main expansion at a distance of approximately 3 mm beyond the faceplate of the main valve. Taking nozzle length (3.5 mm) into account, this corresponds to about 13 nozzle diameters downstream. Minimizing this distance has proven to be crucial to the ideal performance of this anion source, both in

optimizing for spatial constraints and physical properties of the gas expansion. While shorter distances (less than 3 mm) still allow plasma entrainment and might be desired, the body of the main valve faceplate begins to intrude and thus limits the anion signal intensity. Entrainment is also still possible at distances further than 3 mm, but there is diminished collisional cooling which substantially reduces the ability of this new source to produce the species described in Sec. III.

While the necessary conditions for the best overall performance of this anion source have already been discussed (e.g., side valve performance and distance between valves), there are several other variables that change with each experiment. For the preparation of the desired anions, a suitable gas mixture is crucial, as is an appropriate discharge voltage. In each of the following applications, these variables have been optimized and are reported.

III. RESULTS AND DISCUSSION

A. Anion solvation: $OH^-(Ar)_n$

The new source is readily and reproducibly able to solvate anions efficiently and with ample signal intensity to then use in photoelectron imaging experiments. In this experiment, OH^- is formed in a discharge of 1% O_2 and 25% H_2 in Ar at a total pressure of 55 psig, with −2000 V applied to the discharge for 40-140 μs. With a main expansion of neat Ar (40 psig), large $OH^-(Ar)_n$ clusters are easily formed, where OH^- can be solvated by more than 40 Ar atoms. Figure 4 shows a composite mass spectrum of Ar-tagged OH^-, $OH^-(Ar)_n$, ranging from 0 to 29 Ar atoms. Below m/z = 50, there are three predominant peaks: O^-, OH^-, and O_2^-. These ions are formed in the discharge source and drawn into the main expansion of neat Ar. Once in the main expansion, some of the OH^- anions cluster with Ar atoms generating $OH^-(Ar)_n$. The peaks for n = 12 and 18 are prominent, suggesting that 12 and 18 are "magic numbers" that indicate a particularly stable cluster geometry.[42,43] The same magic numbers are also observed in $O^-(Ar)_n$ and correspond to the closing of the solvation shell in an icosahedral (12 Ar atoms) and double icosahedral (18 Ar atoms) structure.[24] Similar solvation shell arrangements likely account for the peak intensities observed for n = 12 and 18 in the $OH^-(Ar)_n$ mass spectrum.

Prior to using this ion source, OH^- was unable to be solvated with more than three Ar atoms using an electron gun source in this laboratory. This new source vastly improves the ability to cool the expansion, making it possible for more than 40 Ar to solvate OH^-. Various gas mixtures of N_2O/CH_4/Ar, N_2O/H_2/Ar, and O_2/CH_4/Ar have been attempted for OH^- production; however, in all cases, the discharge of these gas mixtures produces OH^- intensities that are less intense than the O_2/H_2/Ar mixture. Furthermore, for these other mixtures, many N_2O– or CH_4–solvated anionic complexes, e.g., $OH^-(N_2O)_n$ or $OH^-(CH_4)_n$, also form and result in an undesirable background.

The large cluster anion signal intensity formed from this ion source allows for the photoelectron spectra to be determined for $OH^-(Ar)_n$ as a function of the degree of solvation for the first time. Figure 5 shows a series of photoelectron
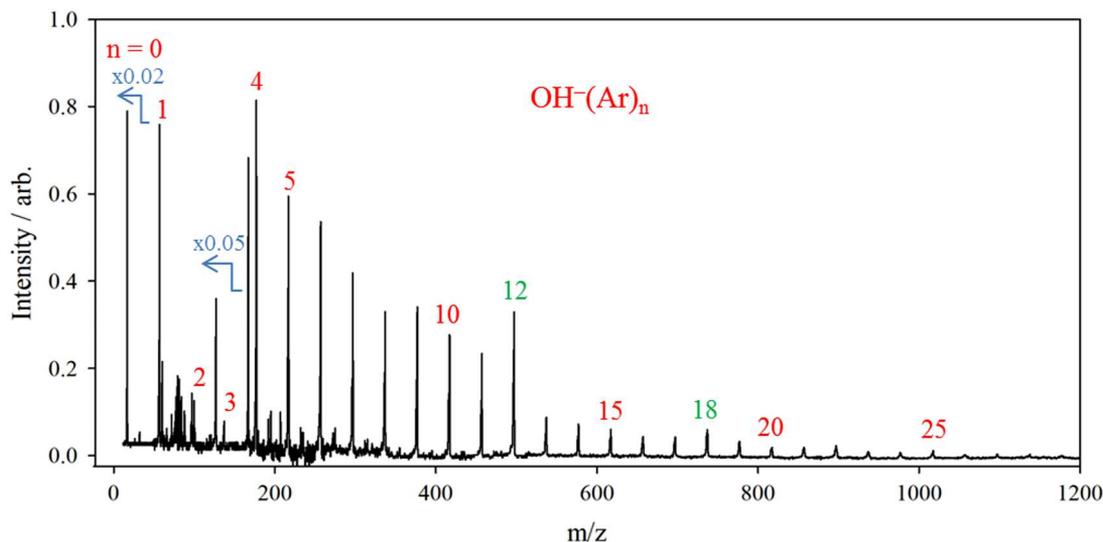
FIG. 4. Composite mass spectrum of $OH^-(Ar)_n$. The small cluster sizes are scaled down as marked in order to view the large cluster distribution and "magic numbers" at n = 12 and 18 (labeled in green). While this mass spectrum only shows out to n = 29, this anion source is able to solvate OH^- with over 40 Ar atoms.

spectra for $OH^-(Ar)_n$ clusters with n = 0, 1, 2, 3, 7, 12, and 18, obtained using three different photodetachment wavelengths: 459 (2.703 eV), 532 (2.330 eV), and 602 (2.060 eV) nm. In the photoelectron spectrum of isolated OH^-, the rotational
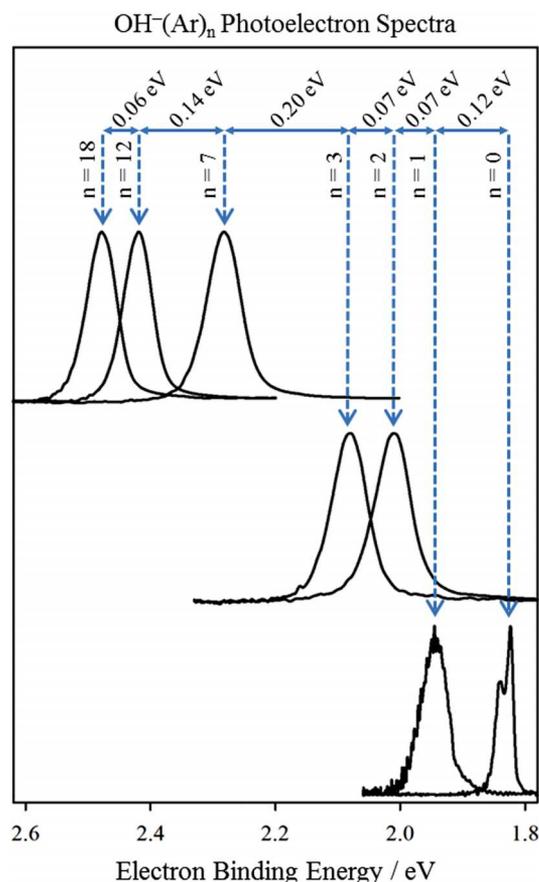
FIG. 5. Photoelectron spectra of $OH^-(Ar)_{n=0,1,2,3,7,12, \text{ and } 18}$ at three different wavelengths: 459 (top), 532 (middle), and 602 (bottom) nm. The solvation energy, indicated above, is derived from peak shift upon further solvation.

branches of the OH radical in the $^2\Pi_{3/2}$ and $^2\Pi_{1/2}$ states are resolved. In the spectra for all of the complexes, there is a single broad peak that shifts to higher electron binding energy as the number of Ar atoms increases. The peak shift is a result of the greater binding energy of the solvent to the anionic cluster than to the neutral cluster. Solvation by the first Ar atom increases the electron binding energy by about 0.12 eV. The next two consecutive Ar additions (n = 2 and 3) each shift the vertical detachment energy (VDE) by about 0.07 eV. The solvation energies (magnitude of the VDE shift) for the various cluster sizes studied are shown in Fig. 5, and demonstrate that the average solvation energy per Ar atom decreases as the cluster size increases. Since Ar atoms in outer solvation shells interact less with the localized negative charge, the addition of Ar atoms beyond n = 12 only shifts the VDE minimally; in fact, the difference in the VDE of n = 12 and n = 18 is only ∼0.06 eV, suggesting an average size-dependent binding energy of 10 meV per Ar atom. This solvation behavior is consistent with studies of $I_2^-(Ar)_n$ and $O^-(Ar)_n$ clusters.[24,27] The diatomic anion is formed from a chemical reaction within the hot, violent environment of the discharge source, but the successful entrainment of the plasma into the main Ar expansion efficiently cools the anions to the point where these very weakly bound complexes (less than 10 meV per Ar on average at the largest cluster sizes studied) are efficiently formed.

Solvation and tagging of ions are important to many areas of physical chemistry. For example, efficient means of producing cold solvated anions has been pursued as a bridge between isolated and bulk (aqueous) systems to better understand the role of the solvent in chemical reaction dynamics. A significant contribution of this new source is to efficiently generate, collisionally cool, and solvate diatomics, triatomics, and larger species with a range of solvents, such as Ar or H_2O.[44] In addition, vibrational predissociation spectroscopy uses weakly bound species, such as Ar or H_2, as a messenger or a "tag" for an ion of interest. By monitoring the loss of the weakly bound species as a function of infrared photon energy,

a vibrational predissociation spectrum of the ion is recorded. With the aid of electronic structure calculations and modeling, the spectroscopic signatures observed can help identify and characterize the structure of the ion of interest. First recorded using predissociation of H_2–solvated species as a function of photon energy, it has facilitated the measurement of infrared spectra of cationic clusters in a continuous beam.[45–47] This technique has since been used with great success for a variety of systems, ranging from small ions to larger biomolecules. Most recent ion sources rely on a cryogenic ion trap to generate sufficiently cold ion clusters.[32] This ion source is able to tag larger species, such as $CH_3O^-(H_2)_n$ and $O_3^-(H_2O)_nAr_m$, with Ar or H_2 solvent species. Both of these systems are briefly discussed in the Supplementary Material.[39]

B. Rational anion synthesis: HOCO⁻

With a cold $OH^-(Ar)_n$ source, as demonstrated in Sec. III A, a well-controlled chemical reaction can facilitate the formation of the anionic forms of OH-containing reaction intermediates that are of interest in atmospheric and combustion chemistry. For example, *cis*– and *trans*–HOCO⁻ are generated in the new ion source through a condensation reaction between neutral CO, present in the main expansion (1% CO in Ar, 40 psig), and OH⁻, formed in the side discharge as in Sec. III A,

$$OH^-(Ar)_{n \geq 0} + CO \rightarrow HOCO^- + nAr,$$
$$\Delta H_{rxn} \approx 0.9\,eV\ (\text{Refs. 48 and 49}).$$
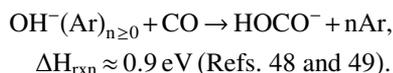
The 764 nm photoelectron spectrum of *cis*– and *trans*–HOCO⁻ is shown as the green trace in Fig. 6. Previously, Johnson *et al.* coupled a cryogenic ion trap to a photoelectron-photofragment coincidence spectrometer for storing and cooling of HOCO⁻ anions in a ~20 K environment.[30,49] Their near-threshold spec-

trum (775 nm) is reproduced as the blue trace in Fig. 6.[49] Comparison of the two spectra conclusively identifies and illustrates the success of the rational anion synthesis of HOCO⁻ in the new ion source.

In addition, the lack of vibrational hot bands from the new ion source demonstrates the ability of this source to efficiently cool isolated (unsolvated, not Ar-tagged) polyatomic anions, despite being formed through an exothermic (by nearly 0.9 eV[48,49]) chemical association reaction. The association reaction takes place in the high density region early in the expansion and subsequent collisions of the anion with Ar result in internally cold HOCO⁻. Bond forming and collisional cooling are likely made possible by taking place in the dense collisional region of the main expansion. However, it is also possible that the initial step in this mechanism contains an association mechanism of $OH^-(Ar)_n$ + CO, where the excess energy from the exothermic bond forming process is funneled into boiling off the weakly bound Ar solvent molecules, allowing the newly formed transient species to stabilize. An additional rational anion synthesis experiment was tested using the new anion source, generating CH_3OO^- through the exothermic association reaction of CH_3^- with O_2 and is briefly discussed in the Supplementary Material.[39]

The adiabatic electron affinities (EAs) of *cis*– and *trans*–HOCO are determined to be 1.511(5) and 1.381(5) eV. This is consistent with, although more precise than, what was previously determined with the aid of modeling, where the EAs of *cis*– and *trans*–HOCO are reported as 1.51(1) and 1.38(1) eV, respectively.[49] The spectrum from this work also has a larger contribution from the *trans*–HOCO⁻ isomer than the previous data. The different proportions of the two isomers are likely due to the way in which the anions are formed. In the previous experiment, the HOCO⁻ anions are stored in the ion trap for several hundred milliseconds where most would likely be quenched to the global minimum, *cis*–HOCO⁻. In the new plasma entrainment source, however, the two isomers are suddenly cooled to their individual minima and are in a collisionless region shortly thereafter, "trapping" proportionally more *trans* isomers.

IV. CONCLUSIONS

A versatile, pulsed anion source that utilizes a plasma-entrainment method suitable for production of cold anions has been developed. This novel setup is capable of solvating or tagging anions with weakly bound Ar atoms to ensure that the internal energy of the ions is low. For example, large ion intensities of $OH^-(Ar)_n$ allow for the solvation energy to be determined for several cluster sizes, where Ar is bound by 10 meV on average in the largest cluster sizes investigated. Further, this ion source is able to produce cold anions through a well-controlled ion-molecule reaction, as demonstrated by the production of HOCO⁻ via association reaction. Additional proof-of-principle experiments demonstrate the versatility of this anion source to be used in the investigation of many cold exotic or transient species, solvated complexes, as well as Ar or H_2 tagged anions. While no experiments were attempted here, this device should be at least as effective when operated as a cation source.
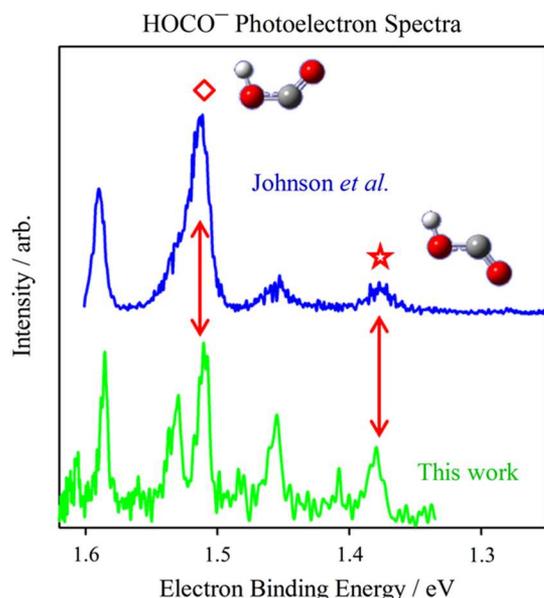
FIG. 6. Comparison of the photoelectron spectra of HOCO⁻ between the 764 nm spectrum (this work, green) and the 775 nm spectrum (blue) from Johnson *et al.*[49] The diamond and star symbols denote the EA of *cis*– and *trans*–HOCO, respectively, from the assignments in the work of Johnson *et al.*[49]

ACKNOWLEDGMENTS

[1]K. M. Ervin and W. C. Lineberger, in *Advances in Gas Phase Ion Chemistry*, edited by N. G. Adams and L. M. Babcock (JAP Press, Greenwich, 1992), Vol. 1, p. 121.

[2]D. M. Neumark, J. Phys. chem. A **112**, 13287 (2008).

[3]A. Sanov and R. Mabbs, Int. Rev. Phys. Chem. **27**, 53 (2008).

[4]R. Mabbs, K. Pichugin, and A. Sanov, J. Chem. Phys. **122**, 174305 (2005).

[5]M. T. Zanni, B. J. Greenblatt, A. V. Davis, and D. M. Neumark, J. Chem. Phys. **111**, 2991 (1999).

[6]B. J. Greenblatt, M. T. Zanni, and D. M. Neumark, Science **276**, 1675 (1997).

[7]N. J. Kim, D. H. Paik, and A. H. Zewail, J. Chem. Phys. **118**, 6930 (2003).

[8]R. Wester, A. E. Bragg, A. V. Davis, and D. M. Neumark, J. Chem. Phys. **119**, 10032 (2003).

[9]L. R. McCunn, G. H. Gardenier, T. L. Guasco, B. M. Elliott, J. C. Bopp, R. A. Relph, and M. A. Johnson, J. Chem. Phys. **128**, 234311 (2008).

[10]L. Sheps, E. M. Miller, S. Horvath, M. A. Thompson, R. Parson, A. B. McCoy, and W. C. Lineberger, Science **328**, 220 (2010).

[11]J. R. Verlet, A. Kammrath, G. B. Griffin, and D. M. Neumark, J. Chem. Phys. **123**, 231102 (2005).

[12]M. A. Johnson and W. C. Lineberger, in *Techniques for the Study of Ion Molecule Reactions*, edited by J. M. Farrar and J. W. Saunders (Wiley, New York, 1988), p. 591.

[13]D. W. Boo, Y. Ozaki, L. H. Andersen, and W. C. Lineberger, J. Phys. Chem. A **101**, 6688 (1997).

[14]E. Garand, T. I. Yacovitch, and D. M. Neumark, J. Chem. Phys. **130**, 064304 (2009).

[15]X. Li, A. Grubisic, S. T. Stokes, J. Cordes, G. F. Ganteför, K. H. Bowen, B. Kiran, M. Willis, P. Jena, R. Burgert, and H. Schnöckel, Science **315**, 356 (2007).

[16]D. L. Osborn, D. J. Leahy, D. R. Cyr, and D. M. Neumark, J. Chem. Phys. **104**, 5026 (1996).

[17]O. Cheshnovsky, S. H. Yang, C. L. Pettiette, M. J. Craycraft, Y. Liu, and R. E. Smalley, Chem. Phys. Lett. **138**, 119 (1987).

[18]L.-S. Wang, H.-S. Cheng, and J. Fan, J. Chem. Phys. **102**, 9480 (1995).

[19]J. M. Weber, Rev. Sci. Instrum. **76**, 043301 (2005).

[20]W. Zheng, S. Xu, D. Radisic, S. Stokes, X. Li, and K. H. Bowen, J. Chem. Phys. **122**, 101103 (2005).

[21]W. H. Robertson and M. A. Johnson, Annu. Rev. Phys. Chem. **54**, 173 (2003).

[22]W. H. Robertson, J. A. Kelley, and M. A. Johnson, Rev. Sci. Instrum. **71**, 4431 (2000).

[23]J. H. Hendricks, H. L. de Clercq, C. B. Freidhoff, S. T. Arnold, J. G. Eaton, C. Fancher, S. A. Lyapustina, J. T. Snodgrass, and K. H. Bowen, J. Chem. Phys. **116**, 7926 (2002).

[24]S. T. Arnold, J. H. Hendricks, and K. H. Bowen, J. Chem. Phys. **102**, 39 (1995).

[25]C. L. Adams, H. Schneider, K. M. Ervin, and J. M. Weber, J. Chem. Phys. **130**, 074307 (2009).

[26]C. L. Adams and J. M. Weber, J. Chem. Phys. **134**, 244301 (2011).

[27]K. R. Asmis, T. R. Taylor, C. Xu, and D. M. Neumark, J. Chem. Phys. **109**, 4389 (1998).

[28]E. M. Miller, L. Sheps, Y.-J. Lu, A. S. Case, A. B. McCoy, and W. C. Lineberger, J. Chem. Phys. **136**, 044313 (2012).

[29]C. Hock, J. B. Kim, M. L. Weichman, T. I. Yacovitch, and D. M. Neumark, J. Chem. Phys. **137**, 244201 (2012).

[30]C. J. Johnson, B. B. Shen, B. L. J. Poad, and R. E. Continetti, Rev. Sci. Instrum. **82**, 105105 (2011).

[31]K. R. Asmis and D. M. Neumark, Acc. Chem. Res. **45**, 43 (2012).

[32]M. Z. Kamrath, R. A. Relph, T. L. Guasco, C. M. Leavitt, and M. A. Johnson, Int. J. Mass Spectrom. Ion Processes **300**, 91 (2011).

[33]T. R. Rizzo, J. A. Stearns, and O. V. Boyarkin, Int. Rev. Phys. Chem. **28**, 481 (2009).

[34]X.-B. Wang and L.-S. Wang, Rev. Sci. Instrum. **79**, 073108 (2008).

[35]L. Sheps, E. M. Miller, and W. C. Lineberger, J. Chem. Phys. **131**, 064304 (2009).

[36]D. W. Chandler and P. L. Houston, J. Chem. Phys. **87**, 1445 (1987).

[37]A. T. J. B. Eppink and D. H. Parker, Rev. Sci. Instrum. **68**, 3477 (1997).

[38]V. Dribinski, A. Ossadtchi, V. A. Mandelshtam, and H. Reisler, Rev. Sci. Instrum. **73**, 2634 (2002).

[39]See Supplementary Material at http://dx.doi.org/10.1063/1.4906300 for detailed schematics of the discharge assembly and general upkeep instructions, as well as additional proof-of-principle experiments.

[40]K. Luria, W. Christen, and U. Even, J. Phys. Chem. A **115**, 7362 (2011).

[41]L. J. Puckett and W. C. Lineberg, Phys. Rev. A **1**, 1635 (1970).

[42]S. R. Desai, C. S. Feigerle, and J. C. Miller, J. Chem. Phys. **97**, 1793 (1992).

[43]O. Echt, K. Sattler, and E. Recknagel, Phys. Rev. Lett. **47**, 1121 (1981).

[44]J. H. Lehman and W. C. Lineberger, J. Chem. Phys. **141**, 154312 (2014).

[45]M. Okumura, L. I. Yeh, and Y. T. Lee, J. Chem. Phys. **83**, 3705 (1985).

[46]M. Okumura, L. I. Yeh, J. D. Myers, and Y. T. Lee, J. Chem. Phys. **85**, 2328 (1986).

[47]M. Okumura, L. I. Yeh, J. D. Myers, and Y. T. Lee, J. Phys. Chem. **94**, 3416 (1990).

[48]J. Li, Y. M. Wang, B. Jiang, J. Y. Ma, R. Dawes, D. Q. Xie, J. M. Bowman, and H. Guo, J. Chem. Phys. **136**, 041103 (2012).

[49]C. J. Johnson, M. E. Harding, B. L. J. Poad, J. F. Stanton, and R. E. Continetti, J. Am. Chem. Soc. **133**, 19606 (2011).